Hindawi
Advances in Civil Engineering
Volume 2022, Article ID 8565125, 16 pages
https://doi.org/10.1155/2022/8565125

Research Article

Seismic Behaviour of Hybrid Precast Shear Walls with Partially Connected Vertically Distributed Reinforcements

Henglin Lv,[1,2,3] **Yuanzhou Wu**,[1,2,3] **Xiongshi Hu**,[4] **Cancan Huang**,[2] **and Kefang Liu**[5]

[1]*Jiangsu Key Laboratory of Environment Impact and Structure Safety in Engineering, China University of Mining and Technology, Xuzhou 221116, China*
[2]*School of Mechanics and Civil Engineering, China University of Mining and Technology, Xuzhou 221116, China*
[3]*JiangSu Collaborative Innovation Centre for Building Energy Saving and Construction Technology, Jiangsu Vocational Institute of Architectural Technology, Xuzhou 221116, China*
[4]*Xuzhou Housing Expropriation and Property Security Management Centre, Xuzhou 221116, China*
[5]*Xuzhou Construction Engineering Testing Centre Co., Ltd., Xuzhou 221116, China*

Correspondence should be addressed to Yuanzhou Wu; wyzcumt@126.com

Received 5 July 2022; Accepted 24 August 2022; Published 19 September 2022

Academic Editor: Youjun Ning

This paper presents a joint mode for a vertical grouting sleeve and a partially distributed reinforced composite connection. The seismic performance of four hybrids precast shear walls with a shear span ratio of 1.83, an axial compression ratio of 0.20, and partially connected vertically distributed rebar was studied by pseudo-static tests. The connection ratios of the reinforced concrete with a vertical distribution were 100%, 67%, 50%, and 33% and were compared with cast-in-place shear walls. It was found that both the precast and cast-in-place specimens demonstrated bending and shear failure modes. Both ends of the mortar layer were cracked under compression, and steel connection failure occurred under the ultimate load. The load-displacement hysteresis curve was bow-shaped and relatively full; the yield load increased from 11.4 to 16.6, and the peak load increased from 4.2 to 6.8 compared with those of the cast-in-situ specimen. The strength degradation performance of the precast specimen was slightly weaker than that of the cast-in-place specimen. The ductility coefficient of the precast specimens was approximately 4, and the ultimate displacement angle was between 1/30 and 1/32, which was larger than the limit value of elastic-plastic interlayer displacement of shear wall structures required by the code. The reduction in the number of vertically distributed rebar connections led to a decrease in the bearing capacity, stiffness, ductility, and energy dissipation, but the impact was very small.

1. Introduction

In a precast reinforced concrete shear wall structure, the concrete is discontinuous due to the existence of joints between the precast members, and the crack resistance of the concrete is decreased below its full value, which leads to early cracking of the member structures. The connection of the rebar under stress results in weak joints, which also affects the mechanical performance of the structure. The mechanical performance of these joints directly determines the seismic performance of the whole structure [1]. Therefore, the joint design is the key factor in the design of precast shear wall structures, and it has a direct impact on engineering applications [2].

Khaled [3, 4] found that the precast shear wall structures had enough bearing capacity and toughness and could be used for seismic fortification with an experimental investigation of five different rebar connections, namely, a rebar and angle steel welding connection; a rebar sleeve connection; local unbonded rebar sleeve connection; a rebar sleeve and shear key connection; and a rebar and steel pipe bolt connection at the horizontal connection. Among them, the local unbonded rebar sleeve connection effectively improved the deformation capacity and energy consumption capacity of the joint. Moreover, the anchorage length directly affected the failure form. Reducing the sleeve diameter strengthened the constraint on the cement slurry and then

increased the adhesion [5]. The compression deformation of concrete in the sleeve position can be effectively constrained by the installation of stirrups in the range of the sleeve connection at the bottom of the precast wall, and then the deformation capacity of the precast shear wall can be improved [6, 7].

It was also found that the grouting quality was required to be very high because of the short sleeve connection, and the rebar positioning requirements were also very strict [8–10]. Therefore, the cost of rebar sleeve grouting connections was high, the production requirements were high, and the difficulty was substantial. Therefore, the constrained slurry anchor connection represented by the corrugated pipe grouting anchor connection was also gradually applied to the vertical connection of the precast reinforced concrete shear wall structure. When using a metal corrugated pipe grouting anchor connection, the precast specimens showed the same bearing capacity, deformation capacity, and energy consumption capacity as the cast-in-place specimens. At the same time, due to the effect of the filling wall and the effective constraint of the local cast-in-place belt, the bearing capacity and stiffness of the structure improved [8]. When the corrugated pipe slurry anchor connection was constrained by a rectangular spiral stirrup, both the precast specimen and the cast-in-place specimen had a good deformation ability that met the seismic requirements [9]. However, the indirect force transfer of the rebar paste anchor connection was complex. Moreover, the number of vertical distribution rebars of the shear wall was large, and the diameter was small. It is not only expensive but also difficult to connect each vertical distribution rebar with a slurry anchor.

Based on the research results above, a hybrid precast shear wall connection method is proposed herein. The marginal vertical rebar adopts the hybrid connection mode of the sleeve grouting anchor connection, and the middle vertically distributed rebar adopts the metal corrugated pipe grouting anchor connection. The advantages of different connection methods can be comprehensively used to effectively improve the structural force performance. By densifying the stirrups of the vertical steel connection section, the effective restraint of the concrete of the edge member, the deformation ability of the concrete, the ductility and seismic performance of the shear wall, and the connection performance of the steel bar in the grout anchor area can all be improved. At the same time, the horizontal rebar in the connection section of the vertical rebar is reinforced to enhance the shear capacity of the shear wall. Through pseudo-static testing, the aseismic performance is studied, which can provide a reference for engineering applications.

2. Research Programme

2.1. Raw Material Performance and Concrete Design. Four kinds of HRB400 steel bars with an elastic modulus of $2.06 \times 10^5\ \mathrm{N/mm^2}$ were used in the experiment, and the diameters of the rebar were 8 mm, 10 mm, 14 mm, and 16 mm. The mechanical properties are illustrated in detail in Table 1.

Concrete C35 was employed in this investigation with a mix ratio of cement: water: sand: stone: admixture: admixture = 1 : 0.56 : 2.47 : 3.42 : 0.28 : 0.04. The cube specimens were cast for the investigation with a size of 150 mm ×150 mm × 150 mm, and the compressive strength was 37.7 MPa after 28 days. The strength of the grouting material used for the grout-bolt connection of precast specimens was 86.2 MPa.

2.2. Specimen Design and Fabrication. A total of 5 shear wall specimens were designed for this experiment, including one cast-in-place specimen XJ and 4 prefabricated specimens YZ1~YZ4. The size of the walls was 200 mm 1200 mm × 2000 mm (thickness × length × height), and the size of the base at the bottom was 2500 mm × 500 mm × 400 mm (length × width × height). The thicknesses of the concrete cover on the wall and base were 20 mm and 25 mm, respectively. The steel bars were all double-row distributed, the horizontal and vertical distribution were all HRB400 rebar with a diameter of 10 mm and a space of 200 mm, and the Rachel steel bars had HRB400 rebar with a diameter of 10 mm and a space of 400 mm × 400 mm. The wall end was provided with a structural edge member, which was 250 mm long along the cross-section, with HRB400 rebar with a diameter of 8 mm and a space of 14 mm, and the stirrups were HRB400 rebar with a diameter of 8 mm and a space of 150 mm. The stirrups of the vertical rebar connection section of the precast specimens were HRB400 rebar with a diameter of 8 mm and a space of 100 mm, and the horizontal rebar was HRB400 rebar with a diameter of 10 mm and a space of 100 mm. The sizes of the specimens and rebar are shown in Figure 1, and the assembly process of the precast shear wall is shown in Figure 2.

2.3. Connection Design. When the mixed precast shear wall specimens were designed and assembled, all the vertical rebar sleeve connections were in the edge member area, and the vertical distribution of rebar grouting anchor connections was present. As shown in Table 2, the vertical distribution rebar in the YZ1 specimens was being all connected, and the rebar connection rates in the YZ2, YZ3, and YZ4 walls were 67 percent, 50 percent, and 33 percent, respectively. The upper wall and the base were poured separately, and the base was embedded in the vertical rebar. The grouting sleeve, metal corrugated pipes, and other embedded parts were embedded in the corresponding positions in the lower part of the wall, and then the base and the upper wall were assembled into a whole with the grouting. Between the precast wall and the base was a sitting paste layer with a thickness of 20 mm. The surface connected between the base and the wall was chiseled to reveal the coarse aggregate. Figure 3 shows the form of the grouting anchor connection used in this test.

2.4. Loading and Test Analysis

2.4.1. Loading Device. The experiment was carried out in the structural hall of the State Key Laboratory of Geotechnical

Table 1: Mechanical properties of rebar.

Diameter (mm)	Yield strength f_y /MPa		Ultimate strength f_u/MPa		Rebar yield strain ε_y/(×10−6)	
	Test value	Average	Test value	Average	Test value	Average
	405		620		1966	
8	410	415	620	618	1990	2014
	430		615		2087	
	515		730		2500	
10	440	463	635	660	2136	2249
	435		615		2112	
	415		595		2014	
14	425	422	580	588	2063	2047
	425		590		2063	
16	475	465	625	613	2306	2257

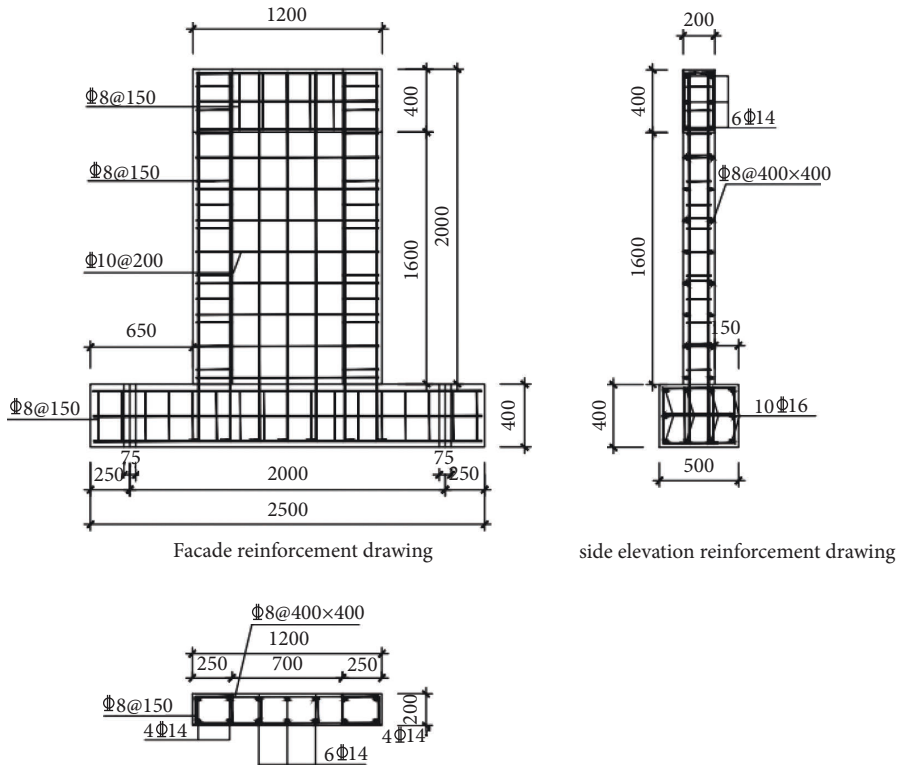

(a)

Figure 1: Continued.

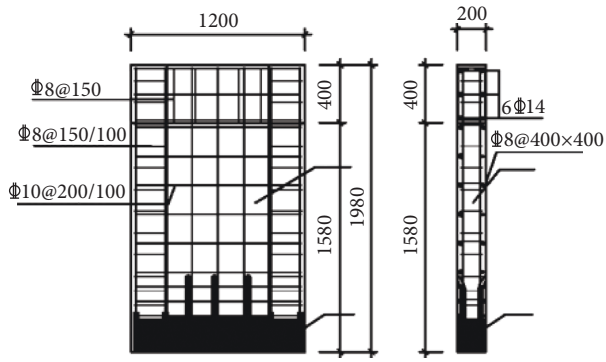

Facade reinforcement drawing of wall side elevation reinforcement drawing of wall

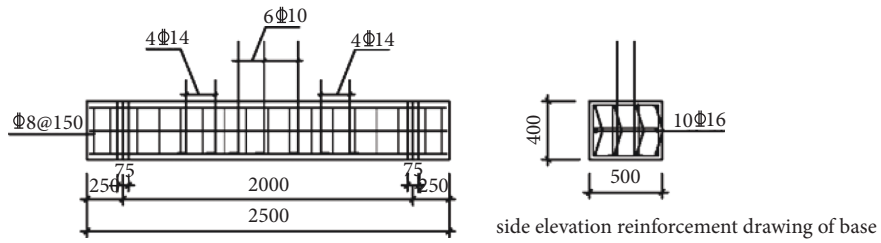

Facade reinforcement drawing of base side elevation reinforcement drawing of base

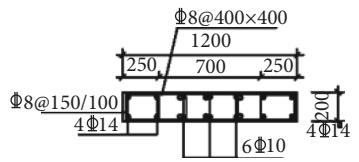

Section reinforcement drawing

(b)

Figure 1: Continued.

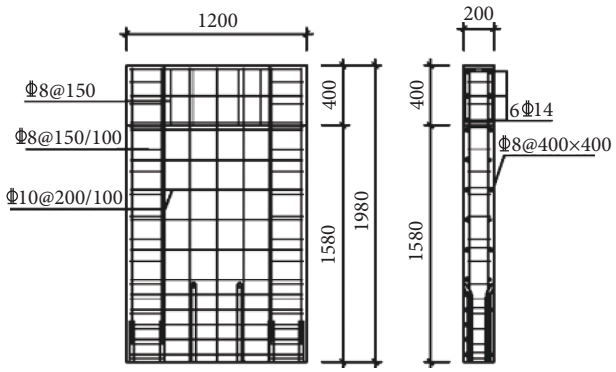

Facade reinforcement drawing of wall side elevation reinforcement drawing of wall

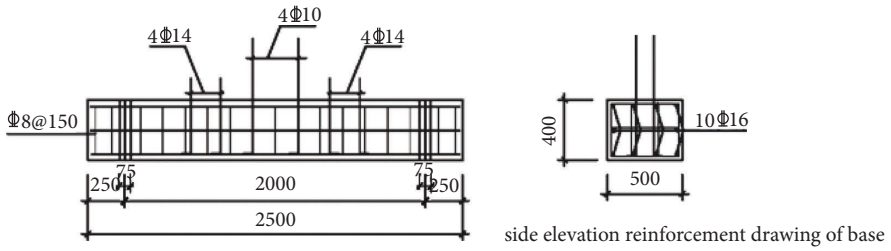

Facade reinforcement drawing of base side elevation reinforcement drawing of base

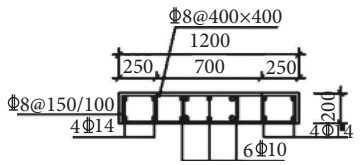

Section reinforcement drawing

(c)

Figure 1: Continued.

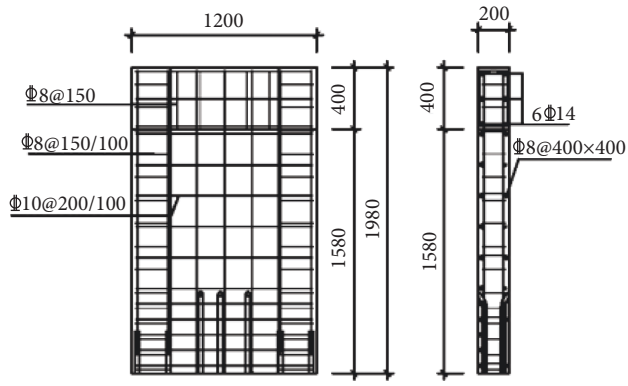

Facade reinforcement drawing of wall side elevation reinforcement drawing of wall

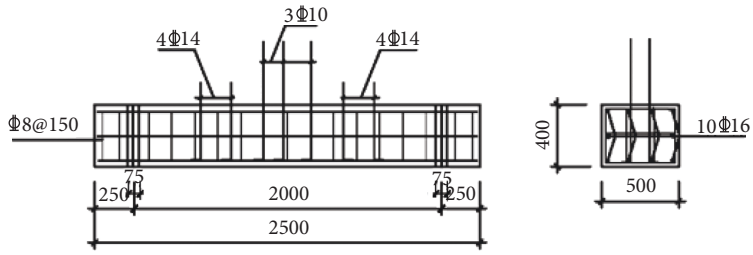

Facade reinforcement drawing of base side elevation reinforcement drawing of base

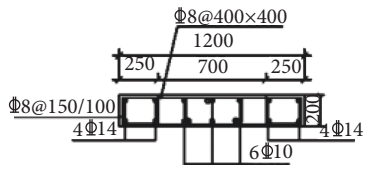

Section reinforcement drawing

(d)

Figure 1: Continued.

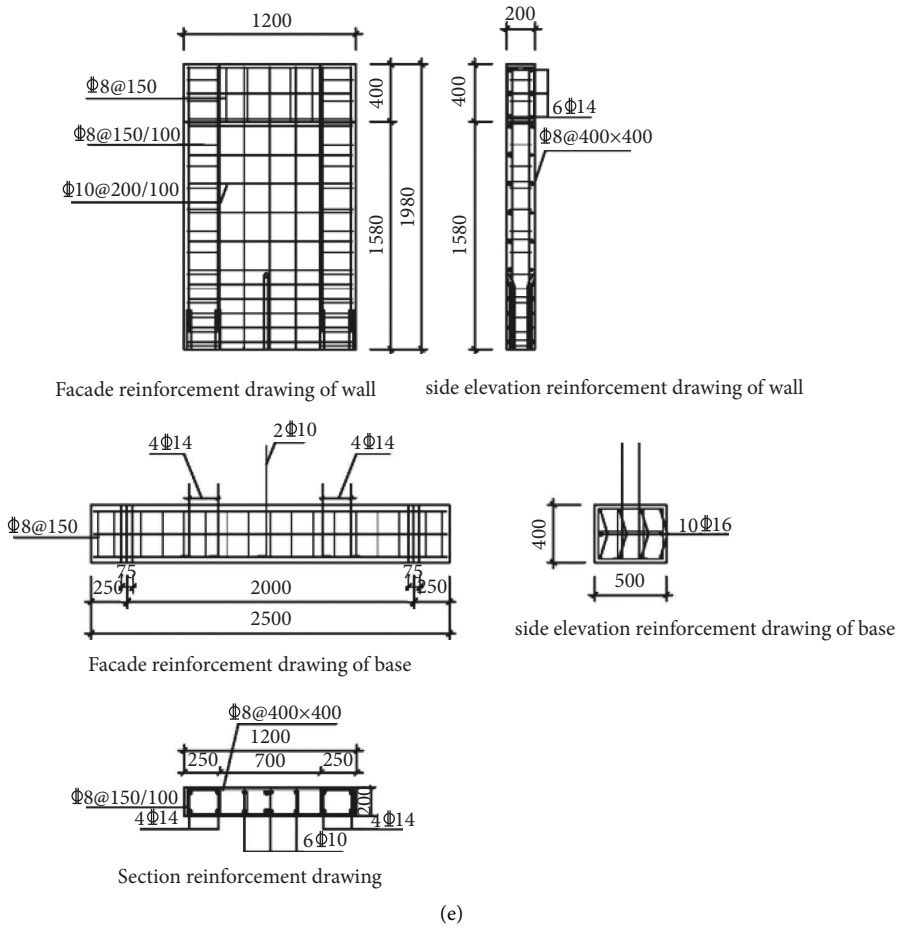

Figure 1: Specimen size and reinforcement drawing. (a) XJ. (b) YZ-1. (c) YZ-2. (d) YZ-3. (e) YZ-4.

Figure 2: Aassembly process of precast shear wall.

and Underground Engineering, China University of Mining and Technology. Figure 4 is a schematic diagram of the loading device.

2.4.2. Loading Scheme. A pseudo-static test was conducted. By controlling the displacement of the loading point of the specimen, the purpose of repeated loading of the specimen was achieved. First, the vertical axial pressure was applied and added to the present value in three equal quantities and kept constant during the test. Then, the horizontal repeated load was applied step by step. First, a forward thrust was applied, and then a reverse tension was applied. The horizontal repeated loading was based on the actual displacement Δ of the wall loading point as the controlled displacement. The control displacement considered the interlayer displacement angle $\theta(\theta = \triangle/H$, where H is the distance from the wall loading point to the base) to have

Table 2: Design parameters of specimen.

NO.	Processing method	Vertical rebar connection mode of edge components	Vertical distributed rebar connection mode	Distributed rebar	Amounts	Distributed rebar connection rate (%)
XJ	Cast-in-place	Through connection	Through connection	HRB400 rebar with the diameter of 10 mm	6	100
YZ1	Precast	Sleeve grouting anchor connection	Metal corrugated pipe grouting anchor connection		6	100
YZ2					4	67
YZ3					3	50
YZ4					2	33

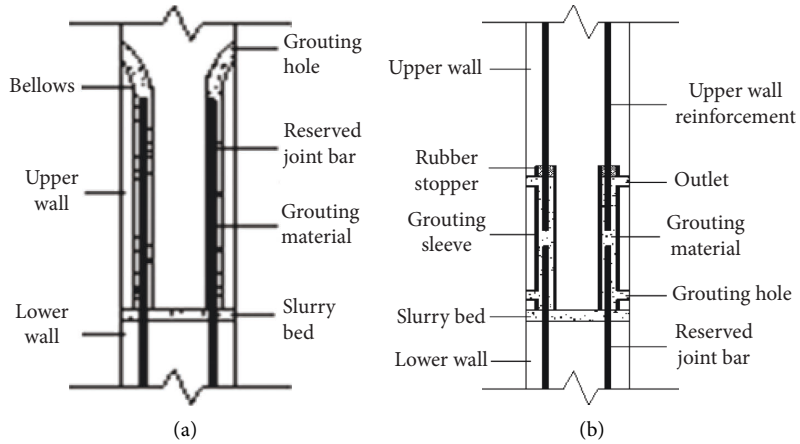

Figure 3: Bolt connection form of specimen. (a) Bellows grout anchor connection. (b) Sleeve grout anchor connection.

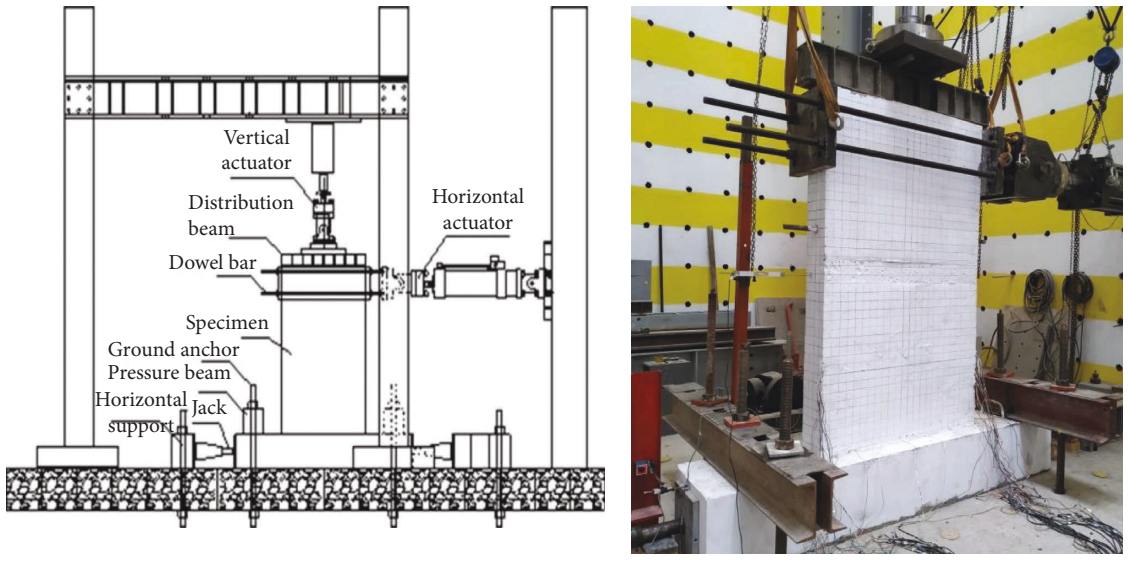

Figure 4: Experimental setup. (a) Schematic. (b) Physical photo.

values of 1/1000, 1/500, 1/300, 1/200, 1/150, 1/120, 1/100, 1/75, 1/60, 1/50, 1/40, and 1/30. It was divided into twelve levels. In addition to the displacement angle of the 1/1000 control displacement single cycle, each control displacement level was repeated three times, for a total of 35 cycles. The test ended when the load dropped below the peak load of 0.85 times or the specimen was destroyed to the point where it was not suitable to continue loading.

The axial pressure N applied by each specimen remained unchanged during the test. The test axial pressure ratio was 0.20, as shown in the following formula:

$$n = \frac{N}{f_{ck}bh}, \tag{1}$$

where $N$is the test shaft pressure, b is the thickness of the specimen, and h is the width of the specimen.

2.4.3. Measurements. The horizontal force and horizontal displacement of the loading point of the wall, the displacement of the pedestal, crack development and distribution, and rebar strain were collected, recorded, and measured as follows:

(a) Load-displacement curves of shear wall loading points: the load and displacement of the load point were collected by the force sensor and displacement sensor on the actuator, respectively.

(b) Base displacement: during the loading process, the displacement of the base was measured by a displacement meter.

(c) Development and distribution of cracks: through the crack observation instrument, we recorded and described the cracks during the process of loading, including the width, position, and shape of the cracks.

(d) Rebar strain: the strain of the tested rebar mainly included vertical rebar, horizontal rebar, and stirrups. The rebar strain was collected in real time by a DH3816 static strain collector. The vertical rebar strain gauges were stuck on the preembedded vertical bars in the base and the vertical rebar in the precast wall. The height of approximately 20 mm from the top of the base and the position of 500 mm from the bottom of the wall was used to judge the force transfer effect. The vertical rebar of the wall, the vertical rebar extending from the base, the stirrup rebar, and the horizontal distribution rebar are referred to as S, D, G, and SP, respectively. The XJ and YZ1 specimen strain gauge arrangements are shown in Figure 5. The strain gauge layout principle of YZ2~YZ4 is the same as that of YZ1 and slightly different in number.

3. Failure Process and Failure Form

3.1. Failure Processes. For specimen XJ, when $\theta = 1/1000$, there was no crack on the wall surface. When $\theta = 1/1500$, cracks appeared on the horizontal joint surface between the slurry layer and the base on the tension side. When $\theta = 1/300$~$1/200$, horizontal cracks appeared in the height range of 600 mm at the bottom of the wall and showed a downward trend. When $\theta = 1/50$~$1/40$, new vertical cracks appeared on the compression side of the bottom of the wall, the concrete protective layer on the bottom edge of the wall collapsed, and the concrete protective layer at the bottom edge of the wall collapsed and delaminated in blocks. The horizontal and longitudinal rebar on both sides of the wall bottom was exposed. At the same time, the longitudinal rebar at the edge of the compression side was bent. The main horizontal cracks on the tension side of the wall reached 2.5 mm. The spalling of concrete at both ends of the bottom caused the concrete on both sides of the bottom to be suspended; when $\theta = 1/30$, the concrete at both ends of the compression side of the wall foot delaminated. At the same time, the vertical rebar on the tensile side was broken, the concrete at the bottom of the wall was almost crushed, and the whole wall suddenly dropped.

When $\theta = 1/1000$, there were no cracks on the surface of the wall; when $\theta = 1/500$, cracks appeared on the horizontal joint surface between the mortar layer and the base on the tension side; when $\theta = 1/200$, horizontal cracks appeared within the height range of 600 mm at the bottom of the wall, which showed a downward trend; and when $\theta = 1/75 \sim 1/60$, there were obvious vertical compression cracks at the bottom of the wall and both sides of the slurry layer, and the concrete at the foot of the wall delaminated in blocks. When $\theta = 1/50 \sim 1/40$, the slurry layer on the tension side started to separate from the upper wall and base, new vertical cracks appeared at the compression side of the wall bottom, large pieces of concrete at the bottom edge of the wall delaminated, the horizontal and longitudinal rebar on both sides of the wall bottom was exposed, and new inclined cracks appeared within the height range of 1400 mm at the bottom of the wall. When $\theta = 1/30$, the vertical steel bar connection on the tensile side of the specimen failed.

3.2. Failure Modes. Both the YZ and XJ specimens show bending shear failure, as shown in Figure 6. The results show that the concrete at both ends of the bottom of the wall collapsed and delaminated, and the rebar was buckled or broken. The inclined cracks extending from the horizontal cracks at the bottom of the wall were the main stress cracks, but the bending shear oblique cracks of the YZ specimen did not develop to the middle part of the wall bottom. The slurry layer of the YZ specimen was the weakest part, and the wall cracks developed gradually from there. Finally, relatively wide horizontal cracks formed in the slurry layer, and both ends of the wall separated from the slurry layer. With the failure of the YZ steel bar connection, the cracks in the upper wall no longer extended upward, and the main cracks were concentrated in a certain range at the bottom of the wall. The failure mode of the YZ specimen was not affected by the connection of the vertical distribution rebar.

3.3. Load-Displacement Hysteresis Curve. Figure 7 shows the load-displacement hysteresis curves from the YZ and XJ specimens. The hysteresis curves of the YZ shear wall specimens and XJ shear wall specimens were very similar, and there was an obvious "pinch shrinkage effect." The overall shape was arched, and the hysteresis curves of the YZ shear wall specimens and XJ shear wall specimens were relatively full, which indicates that the specimens had a good seismic performance.

The hysteresis curve of the YZ specimen was similar to that of the XJ specimen, which can be divided into four stages: cracking, yielding, peak value, and limit. However, at the late stage of loading, the YZ specimens had different degrees of failure in connection with the mortar anchor rebar, resulting in a sudden retraction of the curve. The ultimate bearing capacity of the XJ specimen was smaller than that of the YZ specimen, which proves that strengthening structural measures of the YZ specimen improved the bearing capacity.

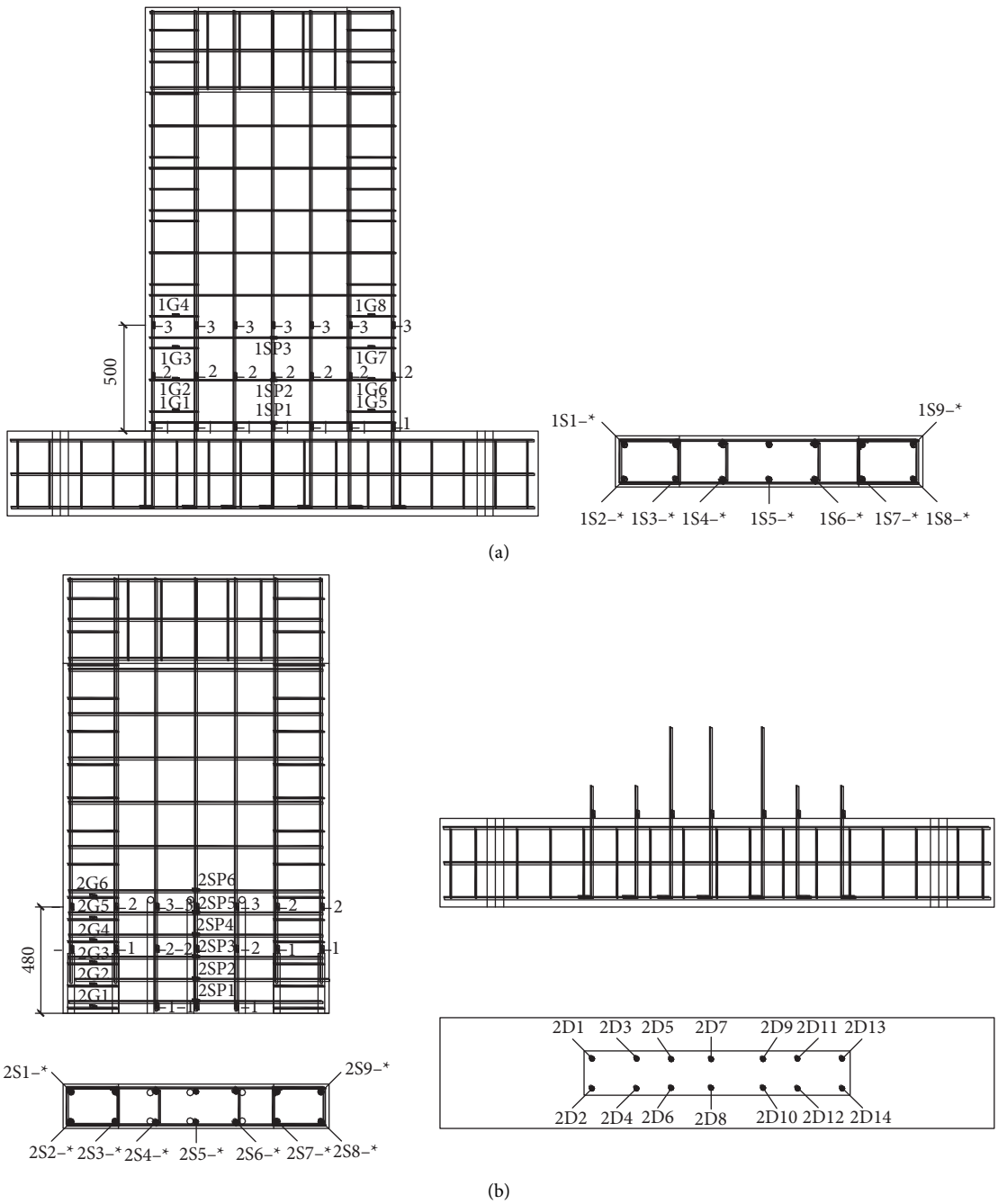

Figure 5: Strain gauge arrangements on specimens of (a) XJ and (b) YZ1.

3.4. Skeleton Curves. The skeleton curves of the YZ and XJ specimens are shown in Figure 8. The overall shapes of the skeleton curves for all specimens were similar, and the trends were the same. In the early stage of loading, the skeleton curves were linear and approximately coincided, which indicates that the stiffness of the YZ and XJ specimens was almost the same. They were in the elastic development stage. With an increase in displacement and cyclic loading of the same displacement, the curve gradually increased to the peak load, and the specimen transitioned into the elastic-plastic stage. After that, the load of the specimen decreased slowly, a stable section appeared, and the YZ and XJ specimens showed good ductility.

Compared with those for the XJ specimen, the YZ specimen had a higher peak bearing capacity, a higher slope, and greater stiffness of the skeleton curve during load growth, which indicates that the stirrup densification of the vertical rebar connection section in the edge member area of the YZ specimen effectively restrained the concrete in the compression zone, prevented premature cracking, and affected the bearing capacity. The overlapping of the distributed rebar in the bottom connection section led to an

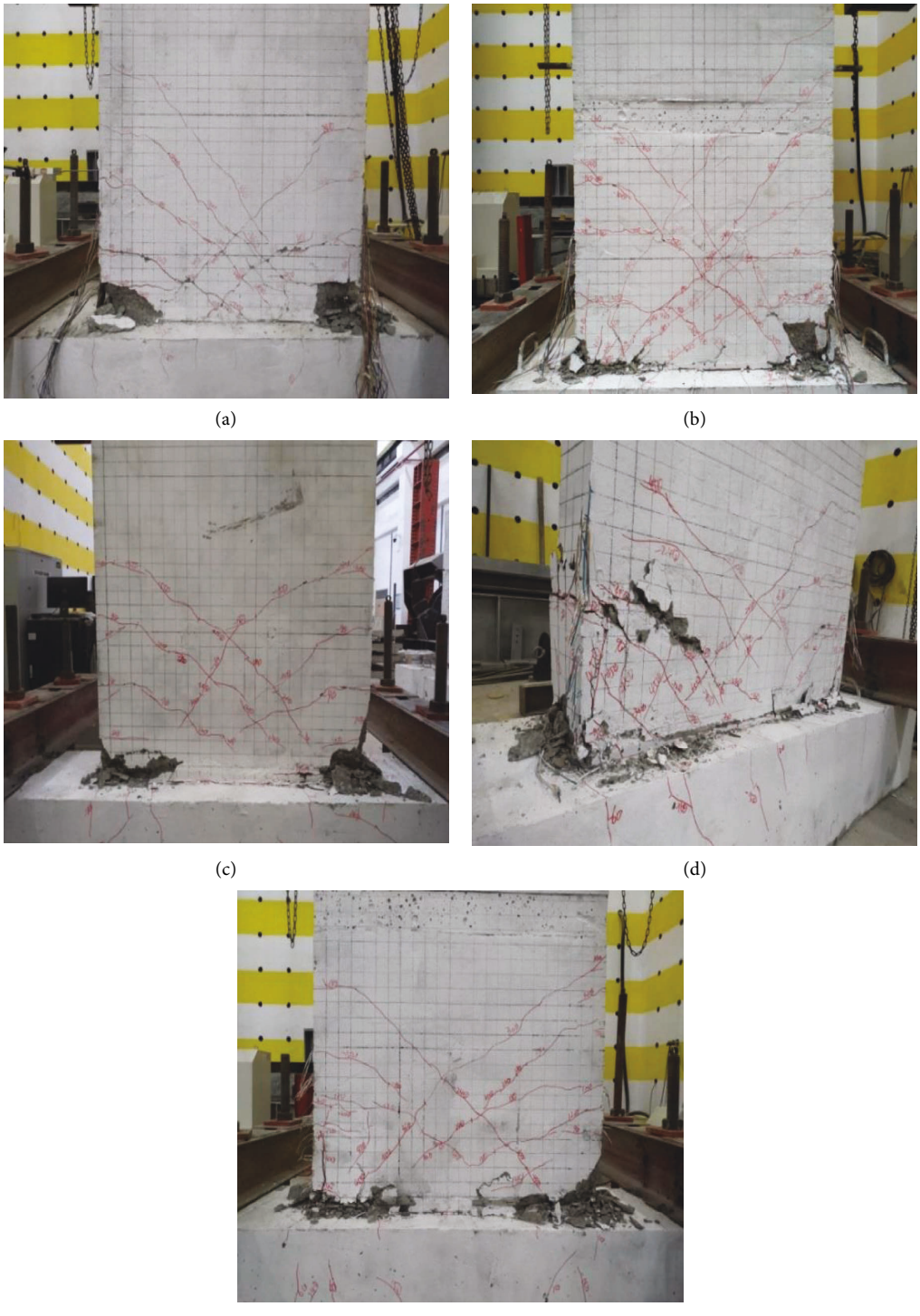

Figure 6: Failure mode and crack distribution. (a) XJ. (b) YZ1. (c) YZ2. (d) YZ3. (e) YZ4.

increase in the rebar in the same section, which effectively improved the bearing capacity of the YZ specimen. Thus, the maximum bearing capacity of the YZ specimen became significantly greater than that of the XJ specimen.

The skeleton curves of the YZ specimens were the same, which shows that the number of partially connected vertically distributed steel bars had little effect on the bearing capacity of the specimens. The peak bearing capacity increased slightly with an increase in the number of vertically distributed steel bars, but the degree of the increase was very small. Table 3 shows a comparison of the bearing capacity test values of the YZ specimen and the XJ specimen.

The yield load and peak load of the YZ specimen were significantly higher than those of the XJ specimen, and the yield load of the YZ specimen ranged from 11.4% to 16.6% higher than that of the XJ specimen. The peak load of the YZ

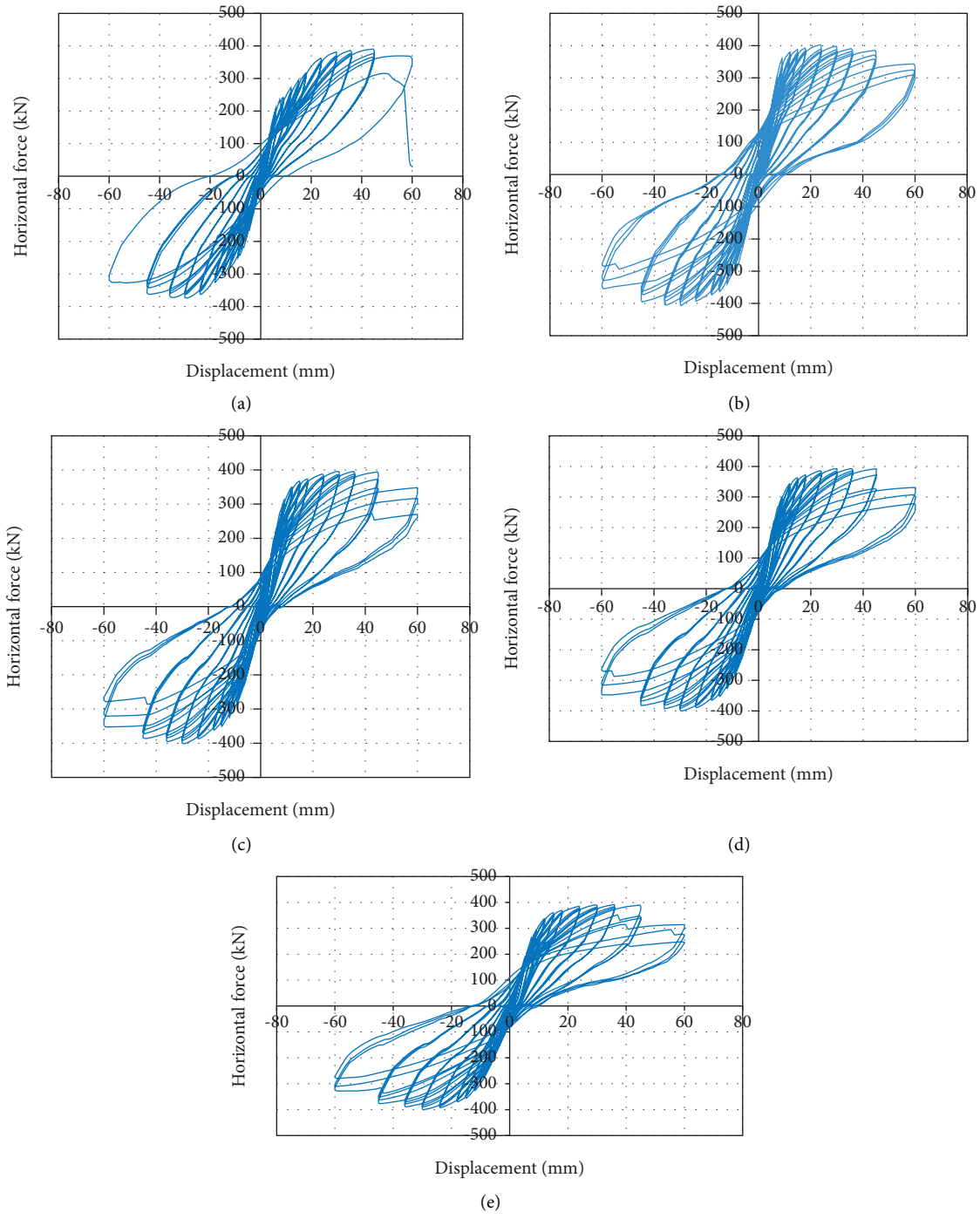

Figure 7: Load-displacement hysteretic curve. (a) XJ. (b) YZ1. (c) YZ2. (d) YZ3. (e) YZ4.

specimen ranged from 4.2% to 6.8% higher than that of the cast-in-place specimen. However, due to the failure of the mortar anchor bar connection, the failure of the YZ specimen was earlier than that of the XJ specimen, and the ultimate load of the YZ specimen was the same as that of the cast-in-place specimen.

The yield load and peak load of the YZ specimens decreased slightly with a decrease in the number of vertically distributed rebar connections. The yield loads of the YZ2, YZ3, and YZ4 specimens were reduced to 95.9%, 95.7%, and 95.6% of the YZ1 specimens, respectively, and the peak loads were reduced to 98.3%, 98.0%, and 97.6%, respectively. The partial connection of the vertically distributed rebar had little effect on the bearing capacity of the YZ specimen.

3.5. Strength Degradation. The load degradation coefficient as a function of the displacement angle of the YZ specimen and XJ specimen at the same level is shown in Figure 9. The curves for the YZ specimen and XJ specimen approximately

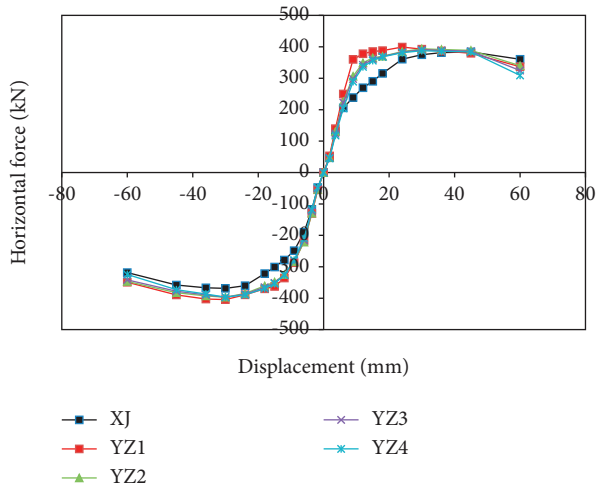

Figure 8: Skeleton curve.

Table 3: Test values of bearing capacity.

Specimen number	F_y(kN)			F_p(kN)			F_u(kN)		
	+	−	Average	+	−	Average	+	−	Average
XJ	318.9	310.2	314.6	383.9	368.7	376.3	360.4	318.5	339.5
YZ1	372.3	361.2	366.8	399.3	404.2	401.8	339.4	349.0	344.2
YZ2	356.2	347.4	351.8	393.5	397.0	395.0	340.0	346.7	343.4
YZ3	351.8	349.9	350.9	390.7	396.8	393.8	332.1	341.8	336.9
YZ4	348.9	352.2	350.6	387.8	396.6	392.2	329.6	337.1	333.4

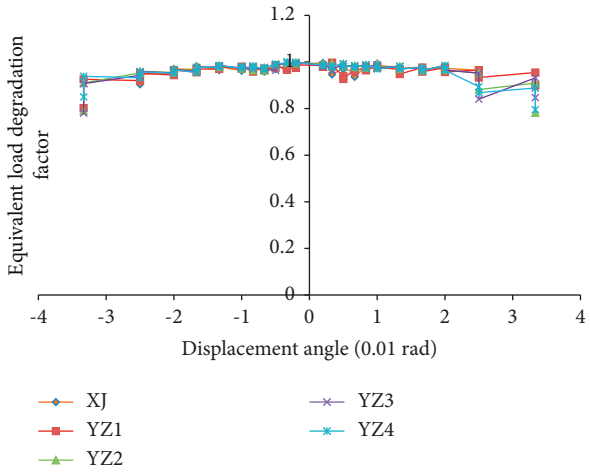

Figure 9: Strength degradation curve.

coincided with each other, and the trend was the same. With an increase in displacement angle, the overall trend was slow and downward, but the degree of the decrease was very small. The load degradation coefficient of the XJ specimen ranged from 0.90 to 1.00 and that of the YZ specimen ranged from 0.78 to 1.00. In the early loading stage of the test, the curves were coincident, and the load degradation coefficients at the same level were almost the same. At the late stage of loading, the degradation coefficient of the same level load of the YZ specimen decreased significantly with an increase in the displacement angle, which was mainly due to the failure of the mortar anchor connection rebar, which resulted in the strength degradation of the YZ specimen being more substantial than that of the XJ specimen.

There was no difference in the load degradation coefficient of the YZ specimen at the same level. During the last two stages of control displacement in the late stage of loading, with a decrease in the number of vertically distributed steel bars, the failure of the reinforced mortar anchor increased substantially, and the load degradation also increased substantially. On the whole, the partial connection of the vertically distributed steel bars had no effect on the load degradation of the specimens.

3.6. Stiffness Degradation. Figure 10 shows the stiffness degradation curves of the YZ and XJ specimens. The stiffness degradation trends for all specimens were consistent, and the shapes were similar. In the early stage of loading, when the specimen was in the elastic working stage, the stiffness of the specimen increased slightly due to the installation gap and then decreased gradually with increasing displacement angle. The stiffness of the specimen decreased rapidly after yielding, and then the curve gradually flattened. At the peak load, the stiffness of the specimen decreased from 44.3% to 50.7% of the initial stiffness. In the late stage, when the displacement angle reached 0.02 rad, the curves gradually approached each other, and the stiffness degradation was gentle.

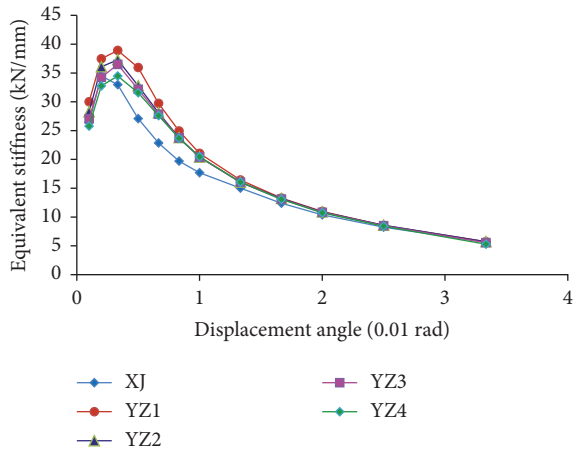

Figure 10: Stiffness degradation curve.

During the test process, the degradation speed of the YZ specimen was slightly less than that of the XJ specimen at the beginning of the specimen stiffness degradation, which indicates that the stirrup density of the vertical rebar connection section in the edge component area of the YZ specimen, the rebar density of the horizontal distribution in the connection section, and the increase in the number of vertical distribution rebar in the same section due to lap connections in the connected section improved the stiffness of the YZ specimen. At the same time, the contribution of the sleeve in the edge member area to the stiffness of the YZ specimen cannot be ignored. With a gradual separation of the mortar layer at the joint of the YZ specimen from the upper wall and base, the stress at the joint increased, and the stiffness degradation degree was more severe than that of the cast-in-place specimen. After loading to the peak displacement, the curve of the specimen tended to be consistent with that of the XJ specimen.

The results show that the stiffness of the YZ specimen increased slightly with an increase in the number of vertically distributed rebar connections, but the overall effect was small. At the same time, before the displacement angle reached 0.01 rad, the stiffness of the YZ specimen decreased slightly with a decrease in the number of vertically distributed rebar connections, but the overall difference was not large. After the displacement angle reached 0.01 rad, the curves of each specimen tended to coincide.

3.7. Ductility. The calculation process of the displacement ductility coefficient of the YZ1 specimen and XJ specimen is shown in Table 4.

The yield displacement angle of the YZ specimen was slightly smaller than that of the XJ specimen, which was mainly because the XJ specimen was whole, while the YZ specimen was connected by a but joint. In the process of loading, the steel bar at the joint was stressed greatly, which led to the early yield of the specimen. The ultimate displacement angles of the YZ and XJ specimens were the same, ranging from 1/30 to 1/32, which was greater than the limit value of 1/120 for the elasto-plastic interstory displacement angle of the shear wall structure under a large earthquake. Both the YZ and XJ specimens meet the ductility requirements.

From the overall trend, it can be seen that the ultimate displacement angle of the YZ specimen was slightly smaller than that of the XJ specimen, which indicates that the YZ specimen entered the failure state ahead of time, and the failure of the mortar anchor connection rebar occurred during the late stage of loading. However, the ductility coefficient of the YZ specimen was slightly higher than that of the XJ specimen. The main reason was that in the late stage of loading, the stirrup densification effectively restrained the large lateral deformation caused by concrete compression. The results show that the ductility of the specimens was improved by properly densifying the stirrups in the vertical rebar connection section and the horizontal distribution rebar in the connection section, which improved the deformation capacity of the YZ specimen.

The yield displacement angles of the YZ specimen differed little, and the ultimate displacement angles of all specimens were the same, which met the requirements of the specification. The ductility coefficient of the YZ specimen was not less than 4, which indicated good ductility. The ductility of the YZ specimen decreased slightly with a decrease in the number of vertically distributed steel bars, which shows that the ductility of the mixed prefabricated shear wall specimens was little affected by the number of connected vertical bars.

3.8. Energy Dissipation Capacity. The cumulative hysteretic energy dissipation of the YZ specimen and XJ specimen with different displacement angles is shown in Figure 11.

The curve of the YZ specimen was consistent with the overall trend of the XJ specimen, and the cumulative hysteretic energy dissipation increased with increasing displacement angle and demonstrated good energy dissipation performance. However, the increasing rate of the cumulative hysteretic energy dissipation curve of the YZ specimen showed a gradually decreasing trend, which was different from the increasing rate of the cumulative hysteretic energy dissipation curve of the XJ specimen. At the initial stage of loading, the cumulative hysteretic energy dissipation curves of the YZ specimen and XJ specimen coincided. When the displacement angle was less than 0.03 rad, the YZ energy dissipation of the specimens was higher than that of the XJ specimen, mainly because the edge component area vertical rebar connection section of the stirrup encryption and encryption strengthened the bottom of the horizontal distribution reinforced connection section. At the same time, due to an increase in the rebar in the same section where the joints overlapped, the mortar anchor connection effectively transferred the force, so the energy dissipation performance of the YZ specimen improved, which led to an improvement in the energy dissipation capacity of the bottom connection area. In the late stage of the experiment, due to the gradual separation of the slurry layer at the horizontal joint of the YZ specimen from the upper wall and base, the growth rate of energy consumption decreased. When the displacement

Table 4: Displacement ductility coefficient.

Specimen number	Δ_y/mm (θ_y/rad)		Δ_u/mm (θ_u/rad)		μ	
	+	−	+	−	+	−
XJ	18.4 (1/98)	16.4 (1/110)	60 (1/30)	60 (1/30)	3.26	3.66
YZ1	11.1 (1/162)	14.8 (1/122)	59.1 (1/30)	60 (1/30)	5.32	4.05
YZ2	13.3 (1/135)	14.9 (1/121)	60 (1/30)	60 (1/30)	4.51	4.03
YZ3	13.5 (1/133)	14.8 (1/122)	58.2 (1/31)	60 (1/30)	4.31	4.03
YZ4	13.9 (1/129)	14.8 (1/122)	55.9 (1/32)	56.1 (1/32)	4.02	3.79

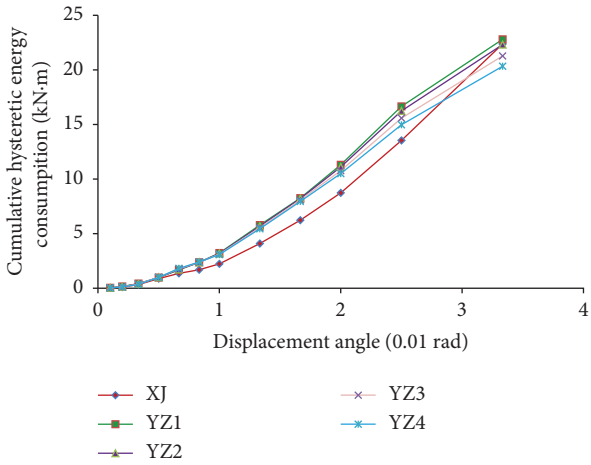

Figure 11: Cumulative hysteretic energy displacement angle relation curve.

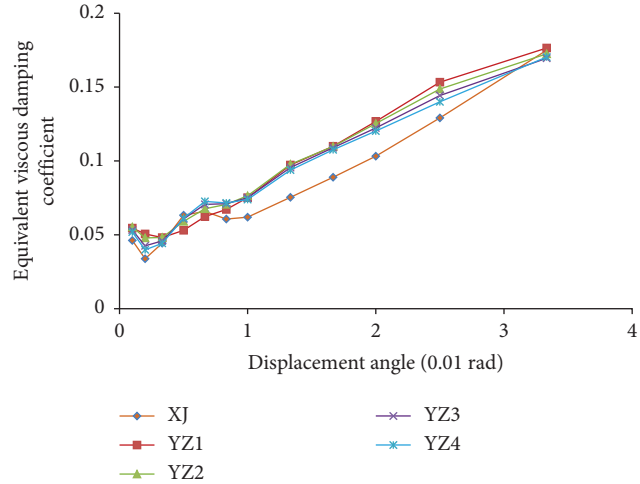

Figure 12: Equivalent viscous damping coefficient curve.

angle reached 0.025 ad, the rebar connection failed, and the cumulative hysteretic energy consumption growth trend decreased significantly and was lower than that of the XJ specimen or had a trend lower than that of the XJ specimen.

The cumulative hysteretic energy consumption of the YZ specimen increased with increasing displacement angle, but the rate of increase gradually slowed. At the early stage of loading, when the displacement angle was less than 0.02 rad, the cumulative hysteretic energy dissipation curves of the specimens were basically coincident. However, at the late stage of loading, due to the gradual separation of the slurry layer at the horizontal joint of the YZ specimen, the upper wall and base, and the gradual failure of the steel bar connection, which led to the growth rate of energy consumption in the late stage of loading slowed. The equivalent viscous damping coefficient curves of the YZ specimen and XJ specimen at different displacement angles are shown in Figure 12.

At the beginning of the test, there was a drop in the equivalent viscous damping coefficient, which was mainly caused by the installation gap between the specimen and the loading device. Then, the curve rose, and when the displacement angle was slightly less than 0.01 rad, the curve exhibited a small decrease because in the early stage of loading, with concrete cracking, the rebar gradually entered the plateau region of the stress-strain curve. Then, most of the steel bars yielded, and the viscous damping coefficient increased steadily with increasing displacement angle. The energy dissipation performance of the YZ specimen was obviously better than that of the cast-in-place specimen, but the growth rate of the overall viscous damping coefficient of the YZ specimen was lower than that of the XJ specimen. When the displacement angle was approximately 0.03 rad, the energy consumption performance of the XJ specimen reached that of the YZ specimen, which was mainly due to the gradual separation of the slurry layer at the horizontal joint from the upper wall and base after loading and the failure of the connection of the mortar anchor rebar. The results show that the energy dissipation performance of the YZ specimens increased slightly with an increase in the number of vertically distributed steel bars, but the overall gap was not obvious.

4. Conclusions

(1) In this paper, a hybrid prefabricated shear wall with partially connected vertically distributed steel bars is proposed. The bearing capacity, stiffness, ductility, and energy dissipation capacity of precast specimens are better than those of cast-in-place specimens, but the strength degradation is slightly lower. The results show that the precast specimens can transfer force effectively before failure, and connection failure occurs under the ultimate load.

(2) The number of connections of vertically distributed steel bars has little influence on the seismic performance of the precast specimens, and all the precast specimens show good seismic performance. Although the reduction of the number of vertically

distributed rebar connections reduces the bearing capacity, stiffness, ductility, and energy consumption of the specimens, the influence is very small.

(3) During the test process, the precast specimens have different degrees of steel failure, resulting in a reduction of the bearing capacity, stiffness, ductility, and energy consumption of the specimens, which can be solved by ensuring the plumpness of the grouting. The specific methods require further research.

Data Availability

All data generated or analyzed during this study are included in this published article.

Conflicts of Interest

The authors declare that they have no conflicts of interest.

Acknowledgments

The authors would like to express their sincere appreciation for the partial financial support by Research Funds for JiangSu Collaborative Innovation Centre for Building Energy Saving and Construction Technology (Contract Number: SJXTZD2102 and SJXTBS2118). The experimental work described in this paper was conducted at the Jiangsu Key Laboratory of Environmental impact and Structural Safety in Civil Engineering in the China University of Mining and Technology. Helps during the testing from staffs and students at the Laboratory are greatly acknowledged. This study was funded by JiangSu Collaborative Innovation Center for Building Energy Saving and Construction Technology Open Fund (Contract Number: SJXTBS2118 and SJXTZD2102).

References

[1] S. Sen and Y. Singh, "Displacement-based seismic design of flat slab-shear wall buildings," *Earthquake Engineering and Engineering Vibration*, vol. 15, no. 02, pp. 209–221, 2016.

[2] J. Sun and H. X. Qiu, "Seismic behavior and mechanism analysis of innovative precast shear wall involving vertical joints," *Journal of Central South University*, vol. 22, no. 4, pp. 1536–1547, 2015.

[3] K. A. Soudki, S. H. Rizkalla, and B. LeBlanc, "Horizontal connections for precast concrete shear walls subjected to cyclic deformations part1: mild steel connections," *PCI Journal*, vol. 40, no. 4, pp. 78–96, 1995.

[4] K. A. Soudki, S. H. Rizkalla, and R. W. Daikiw, "Horizontal connections for precast concrete shear walls subjected to cyclic deformations part2: prestressed connections," *PCI Journal*, vol. 40, no. 5, pp. 82–96, 1995.

[5] H. Jiang, Q. Cao, A. Liu, T. Wang, and Y. Qiu, "Flexural behavior of precast concrete segmental beams with hybrid tendons and dry joints," *Construction and Building Materials*, vol. 110, no. 1, pp. 1–7, 2016.

[6] Y. Y. Peng, J. R. Qian, and Y. H. Wang, "Cyclic performance of precast concrete shear walls with a mortar–sleeve connection for longitudinal steel bars," *Materials and Structures*, vol. 49, no. 6, pp. 2455–2469, 2016.

[7] G. Xu, Z. Wang, B. Wu et al., "Seismic performance of precast shear wall with sleeves connection based on experimental and numerical studies," *Engineering Structures*, vol. 150, no. 1, pp. 346–358, 2017.

[8] Q. Gu, G. Dong, X. Wang, H. Jiang, and S. Peng, "Research on pseudo-static cyclic tests of precast concrete shear walls with vertical rebar lapping in grout-filled constrained hole," *Engineering Structures*, vol. 189, pp. 396–410, 2019.

[9] J.-B. Liu, Y.-G. Chen, Z. X. Guo, and F. Yuan, "Aseismic behavior of precast shear walls with spiral hoop restraint," *Journal of South China University of Technology: Natural Science Edition*, vol. 42, no. 11, pp. 92–98, 2014.

[10] B. Andrea and R. Paolo, "Seismic performance and retrofit of precast concrete grouted steeve connections," *PCI Journal*, vol. 57, no. 1, pp. 97–109, 2012.